The Astrophysical Journal Letters, 739:L30 (5pp), 2011 September 20 doi:10.1088/2041-8205/739/1/L30
© 2011. The American Astronomical Society. All rights reserved. Printed in the U.S.A.

A MOLECULAR EINSTEIN RING TOWARD THE $z = 3.93$ SUBMILLIMETER GALAXY MM18423+5938

Jean-François Lestrade[1], Chris L. Carilli[2], Karun Thanjavur[3,4], Jean-Paul Kneib[5], Dominik A. Riechers[6], Frank Bertoldi[7], Fabian Walter[8], and Alain Omont[9]
[1] Observatoire de Paris, CNRS, 61 Av. de l'Observatoire, F-75014, Paris, France; jean-francois.lestrade@obspm.fr
[2] NRAO, Pete V. Domenici Array Science Center, P.O. Box O, Socorro, NM 87801, USA
[3] Canada France Hawaii Telescope Corporation, HI 96743, USA
[4] Department of Physics & Astronomy, University of Victoria, Victoria, BC, V8P 1A1, Canada
[5] Laboratoire d'Astrophysique de Marseille, Observatoire d'Astronomie Marseille-Provence, BP 8, F13376 Marseille, France
[6] Astronomy Department, Caltech, 1200 East California boulevard, Pasadena, CA 91125, USA
[7] Argelander Institute for Astronomy, University of Bonn, Auf dem Hugel 71, 53121 Bonn, Germany
[8] Max-Planck Institute for Astronomy, Konigstuhl 17, D-69117 Heidelberg, Germany
[9] Institut d'Astrophysique de Paris, 98bis Bld Arago, F75014, Paris, France
Received 2011 April 12; accepted 2011 May 27; published 2011 August 29

ABSTRACT

We present high-resolution imaging of the low-order ($J = 1$ and 2) CO line emission from the $z = 3.93$ submillimeter galaxy (SMG) MM18423+5938 using the Expanded Very Large Array, and optical and near-IR imaging using the Canada–France–Hawaii Telescope. This SMG with a spectroscopic redshift was thought to be gravitationally lensed given its enormous apparent brightness. We find that the CO emission is consistent with a complete Einstein ring with a major axis diameter of $\sim 1\farcs4$, indicative of lensing. We have also identified the lensing galaxy as a very red elliptical coincident with the geometric center of the ring and estimated its photometric redshift $z \sim 1.1$. A first estimate of the lens magnification factor is $m \sim 12$. The luminosity $L'_{\mathrm{CO}(1-0)}$ of the CO(1 − 0) emission is $2.71 \pm 0.38 \times 10^{11}\ m^{-1}$ K km s^{-1} pc^2, and, adopting the commonly used conversion factor for ultraluminous infrared galaxies (ULIRGs), the molecular gas mass is $M(\mathrm{H_2}) = 2.2 \times 10^{11}\, m^{-1}\, M_\odot$, comparable to unlensed SMGs if corrected by $m \sim 12$. Our revised estimate of the far-IR luminosity of MM18423+5938 is $2 \times 10^{13}\, m^{-1} < L_{\mathrm{FIR}} < 3 \times 10^{14}\, m^{-1} L_\odot$, comparable to that of ULIRGs. Further observations are required to quantify the star formation rate in MM18423+5938 and to constrain the mass model of the lens in more detail.

Key words: galaxies: evolution – galaxies: high-redshift – galaxies: ISM – galaxies: starburst – gravitational lensing: strong – submillimeter: galaxies

Online-only material: color figures

1. INTRODUCTION

There is mounting evidence that large ellipical galaxies form the majority of their stars at early epochs ($z > 1$) and quickly (duration <1 Gyr; Renzini 2006). Bright submillimeter-selected galaxies (SMGs; defined as $S_{850\,\mu\mathrm{m}} > 3$ mJy) are an important galaxy population in this regard, likely representing a key star formation epoch with extreme starbursts thought to be driven by major mergers of gas-rich galaxies at high redshift (Smail et al. 2002; Blain et al. 2002; Tacconi et al. 2008). The discovery of evolved galaxies at high redshift ($z > 2$; Daddi et al. 2005; Kriek et al. 2008; Toft et al. 2009; van Dokkum et al. 2008; Kurk et al. 2009; Collins et al. 2009; Williams et al. 2009; Kotilainen et al. 2009), as well as luminous SMGs at even higher redshifts ($z > 5$; Riechers et al. 2010; Capak et al. 2011), provides evidence for this early active star formation phase out to about 1 Gyr after the big bang.

The very bright SMG MM18423+5938 ($S_{1200\,\mu\mathrm{m}} = 30 \pm 3$ mJy) was discovered serendipitously at the Institut de Radioastronomie Millimétrique (IRAM) 30 m telescope with the bolometer array MAMBO (Lestrade et al. 2009). Although no optical counterpart was known for MM18423+5938, its redshift $z = 3.92960 \pm 0.00013$ was spectroscopically measured through the detection of several strong CO and CI emission lines with the wide spectrometer EMIR (Eight Mixer Receiver) also at this telescope (Lestrade et al. 2010). These line detections indicate a massive reservoir of molecular gas in a galaxy only 1.6 Gyr after the big bang. The observed CO ladder (CO(4–3), CO(6–5) and CO(7–6), CO(9–8) upper limit) peaks around $J = 5$, indicative of a starburst-powered SMG that is not dominantly excited by an active galactic nucleus (AGN).

Recently, bright, strongly lensed SMGs have been discovered in large area surveys (Vieira et al. 2010; Negrello et al. 2010; Frayer et al. 2011). Even compared to these, MM18423+5938 is very bright, and its well-established redshift makes it a prime target for high-resolution observations to study the cause of its high brightness, to understand its place in this emerging population, to verify the hypothesis that it is gravitationally lensed, and to study further the similarities of MM18423+5938 with the other very bright SMG SMMJ2135−0102 at $z = 2.3$ ($S_{850\,\mu\mathrm{m}} = 106$ mJy), which has been shown to be strongly lensed (Swinbank et al. 2010).

In this Letter, we report observations of the CO(1–0) and CO(2–1) line emissions in MM18423+5938 to $0\farcs6$ resolution using the Expanded Very Large Array (EVLA; Perley et al. 2011), as well as multicolor optical and near-IR imaging using the Canada–France–Hawaii Telescope (CFHT). These observations confirm that MM18423+5938 is lensed, providing a unique opportunity to study the gas dynamics on small physical scale with further high sensitivity and high spatial resolution EVLA observations. We use a concordance, flat Λ-CDM cosmology throughout, with $H_0 = 71$ km s^{-1} Mpc^{-1}, $\Omega_M = 0.27$, and $\Omega_\Lambda = 0.73$.

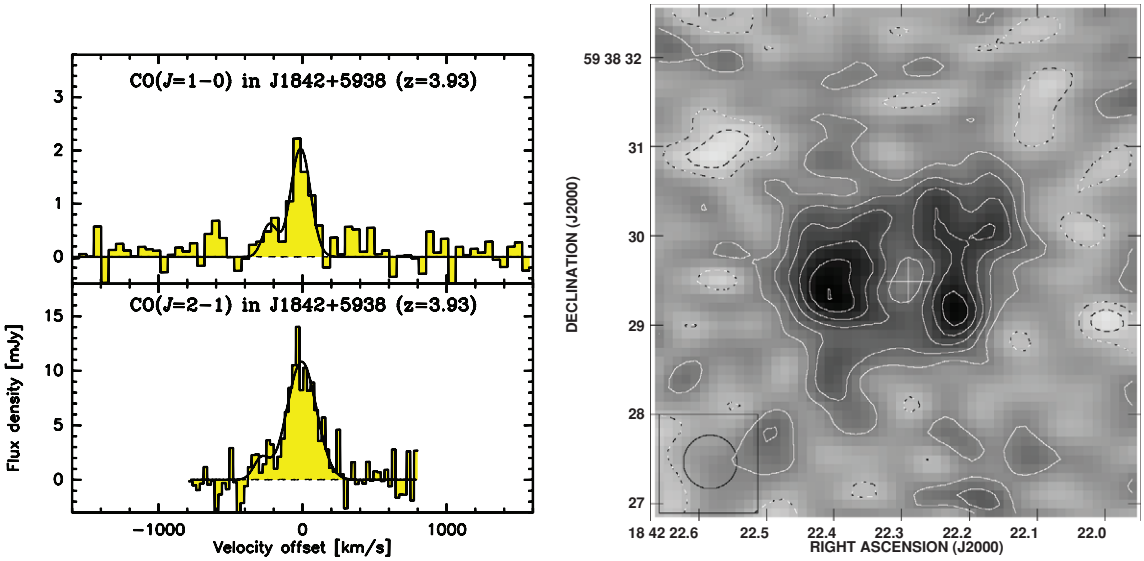

Figure 1. EVLA observations. Top left: spectrum of the CO(1–0) emission from MM18423+5938 at 51 km s^{-1} resolution. Bottom left: spectrum of the CO(2–1) emission at 26 km s^{-1} resolution. Zero velocity corresponds to the redshift $z = 3.9296$. Right: image of the CO(2–1) emission from MM18423+5938 integrated over 230 km s^{-1} at 0.″6 resolution. The rms is 0.16 mJy beam^{-1}, and the contour levels are −0.4, −0.2, 0.2, 0.4, 0.6, 0.8, 1.0, 1.2 mJy beam^{-1}. Negative contours are dashed. The cross shows the position of the lensing galaxy at the ring center.

(A color version of this figure is available in the online journal.)

Table 1
Observed Line Parameters of Two-component Gaussian Fit

Line	S_ν (mJy)	$\Delta V_{\rm FWHM}$ (km s^{-1})	V_0 (km s^{-1})	$I_{\rm CO}$ (Jy km s^{-1})	$L'_{\rm CO}10^{-11}$ (K km s^{-1} pc^2)
CO(1–0)	2.05 ± 0.22	161 ± 30	-14 ± 11	0.35 ± 0.05	2.71 ± 0.38
	0.62 ± 0.38	118 ± 114	-228 ± 52	0.078 ± 0.06	
CO(2–1)	10.83 ± 0.74	239 ± 26	-6 ± 9	2.74 ± 0.23	4.74 ± 0.40
	1.92 ± 1.34	125 ± 128	-286 ± 59	0.25 ± 0.20	

Notes. Zero velocity corresponds to a redshift $z = 3.9296$. The apparent $L'_{\rm CO}$ results from the two components added up. Only statistical uncertainties are given.

2. OBSERVATIONAL DATA AND REDUCTIONS

2.1. Expanded Very Large Array

Observations were made in the C configuration of the EVLA in 2010 December. We targeted the CO(1–0) line (rest frequency = 115.271 GHz) at 23.38 GHz and the CO(2–1) line (rest frequency = 230.538 GHz) at 46.76 GHz. A total bandwidth of 248 MHz was employed, with 124 spectral channels. Spectral imaging of the broad line of MM18423+5938 at high spectral resolution was made possible with the new capability of the WIDAR correlator of the EVLA (Perley et al. 2011). The total observing time was 2 hr at 23 GHz and 8 hr at 47 GHz. Dynamic scheduling was employed to ensure good atmospheric observing conditions. The phase calibrator was J1849+6705 and the switching cycle was 5 minutes (Carilli & Holdaway 1999). The synthesized beam FWHM using robust weighting ($R = 1$) in the AIPS data analysis software was 2.″1 × 1.″0 at 23 GHz, and roughly circular with FWHM = 0.″6 at 47 GHz. The flux density scale was set by observing 3C48, but some observations at 47 GHz were made with the target source and 3C48 at very different elevations. We estimate an absolute calibration uncertainty at 47 GHz of ±20%, even with the nominal opacity correction made using the weather data (Butler 2010). The rms noise per channel is 0.16 mJy beam^{-1} at 23 GHz (rest frequency = 115.271 GHz) at 51 km s^{-1} resolution, and 0.48 mJy beam^{-1} at 47 GHz (rest frequency = 230.538 GHz) at 26 km s^{-1} resolution.

Figure 1 (left panel) shows the CO(1–0) and CO(2–1) spectra. Both lines show a possible non-Gaussian tail toward lower velocities, so two components were fitted to both the CO(1–0) and CO(2–1) profiles. Line peak flux densities, line widths, mean velocities and velocity-integrated line fluxes $I_{\rm CO}$ are in Table 1.

Figure 1 (right panel) shows the CO(2–1) emission integrated over the channels of the full line width (230 km s^{-1}) at 0.″6 resolution. The morphology is consistent with an Einstein ring interpretation. The ring is elliptical, with a major axis ∼1.″4 and a minor axis ∼1.″2. The J2000 coordinates of the ring center (geometric center of the inner hole) are $\alpha = 18^{\rm h}42^{\rm m}22^{\rm s}.29$, $\delta = 59^\circ38'29''.5 \pm 0''.2$ in the International Celestial Reference System (ICRS). No continuum emission is detected at either frequency, with 3σ limits of 75 μJy beam^{-1} at 23 GHz and 210 μJy beam^{-1} at 47 GHz.

2.2. CFHT Optical and Near-IR Imaging

To identify the putative lensing galaxy, we carried out multiband optical and near-IR (NIR) imaging at the CFHT with the prime focus imagers, *MegaCam* and *WIRCam*, respectively. The observations were completed in 2010 November, with total on-source integration times of 4.75 hr on MegaCam (6300 s in *i*,

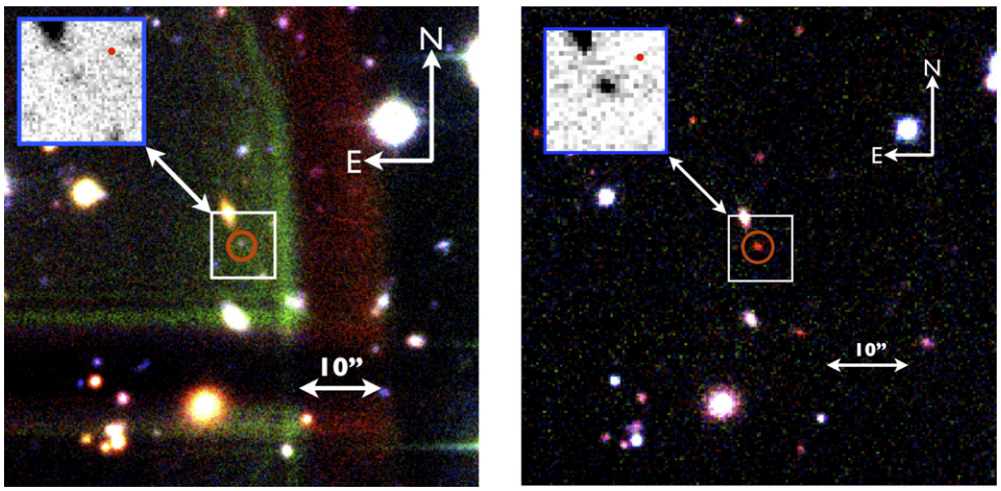

Figure 2. CFHT images. RGB color images of 60″ × 60″ regions centered on MM18423+5938 in the stacked MegaCam *g*, *r*, and *i*, and WIRCam *J*-, *H*-, and *Ks*-band images, respectively, are shown in the left and right panels. The pixel scales are 0.″187 and 0.″304 in the MegaCam and WIRCam images, respectively. The main lens galaxy is circled in red and is at the center of the insets (8″ × 8″). The red dots in the insets are the FWHM point-spread function (PSF) during observations (in *r* band and *Ks* band). The optical image was affected by scattered light from two nearby ∼9 Vmag stars, see Section 2.2 for details.

(A color version of this figure is available in the online journal.)

Table 2
CFHT GRIZ and JHK_S Band Photometry (Extinction Corrected AB Magnitudes)

Object	*g*	*r*	*i*	*z*	*J*	*H*	*Ks*
Lens galaxy	26.33 ± 0.43	24.84 ± 0.20	24.17 ± 0.15	···	21.81 ± 0.24	21.25 ± 0.33	20.74 ± 0.08
Nearby galaxy (N.E.)	23.75 ± 0.05	22.28 ± 0.03	21.33 ± 0.02	20.67 ± 0.04	19.19 ± 0.03	19.14 ± 0.04	19.08 ± 0.02

5400 s in *r*, and 2700 s each in *g* and *z* filters) and 0.58 hr on WIRCam (950 s in *Ks*, 840 s in *J*, and 285 s in *H* bands). The median seeing during the optical imaging was 0.″65 in the *r* band, which was well sampled by the MegaCam pixel scale of 0.″187; during the NIR imaging, the median seeing was 0.″7 in *Ks* band, marginally sampled by the WIRCam 0.″304 pixel scale. Standard calibrations were obtained and the data processed at CFHT with the *Elixir* and *I′iwi v*.2 pipelines. The sky-subtracted dithered exposures in each filter were stacked using *Swarp* (Bertin et al. 2002) and MegaPipe (Gwyn 2008). For obtaining consistent photometry in all passbands, the NIR images were re-convolved from 0.″304 pixel scale to the MegaCam resolution of 0.″187 during stacking of the dithered WIRCam images. Astrometric and photometric calibrations in the optical and NIR were carried out with *Scamp* (Bertin 2006), against USNO-B1 (Monet et al. 2003), and Two Micron All Sky Survey (2MASS) Point Source Catalogs (Skrutskie et al. 2006). The 2MASS positions are tied to the ICRS system via the *Hipparcos Tycho* reference frame to better than 0.″2 (2MASS Explanetary Supplement Chap. I, subsection 6b, paragraph IX). There are thirteen 2MASS sources in our full WIRCam image that have been used for this NIR–radio registration. The RGB color stamp images (Figure 2) constructed with optical *gri* filters, and the NIR *JHKs* bands, show a red galaxy (with ellipticity = 0.19) at $\alpha = 18^{\rm h}42^{\rm m}22^{\rm s}.27 \pm 0''.29$, $\delta = 59^\circ38'29''.6 \pm 0''.25$ in the ICRS, i.e., in the same coordinate system as our EVLA map. In the NIR (Figure 2, right), the detection significance is at 10σ in *Ks* and at $\sim 3\sigma$ in *J* and *H* bands. In the optical (Figure 2, left), the bright stellar halo from the two nearby ∼9 Vmag saturated stars led to significant background noise, and therefore to lower detection significances but nonetheless successful identifications in the *i*, *g*, *r* filters. The *z* filter was affected by fringing.

Given the low detection significances in the optical imaging, magnitudes were measured using *Sextractor* (Bertin & Arnouts 1996) in dual image mode, using the *Ks*-band image for object detection, while measuring the flux in matched apertures in all filters; for the optical filters, the WIRCam *Ks* image was resampled to match the pixel scale of MegaCam. Further, we carried out photometry of the nearby galaxy at $\alpha = 18^{\rm h}42^{\rm m}22^{\rm s}.52 \pm 0''.36$, $\delta = 59^\circ38'33''.17 \pm 0''.31$ in the ICRS (lying 5″ east of north of the putative lens, see Figure 2) expected to contribute to the lensing model. The foreground Galactic extinction corrected *AB*-magnitudes are in Table 2 (extinction $E(B-V)$ is 0.0462 ± 0.0009 at the source position in Schleger maps).

3. ANALYSIS AND DISCUSSIONS

Figure 3 shows an overlay of the CO(2–1) contour map of MM18423+5938 and the *Ks*-band image. The main lens galaxy is coincident with the geometric center of the ring. With the measured NIR and optical magnitudes, we used spectral energy distribution (SED) fitting in *LePhare* (Arnouts et al. 1999) to estimate a photometric redshift $z_{\rm phot} \sim 1.1$, with a formal uncertainty of ±0.1, for the lens best fit with an early type galaxy template. No satisfactory fit was obtained for the northeast nearby galaxy mainly because the *J* magnitude did not match with the other bands. We built a preliminary lens model based on isothermal elliptical potentials for the two galaxies using the *LENSTOOL* Software (Kneib et al. 1996; Jullo et al. 2007). This resulted in a quadruple image with the two brightest spots located at the two maxima of the CO(2–1) map, and yielded the total magnification factor $m \sim 12$. The nearby galaxy contributes to the lensing model in making the

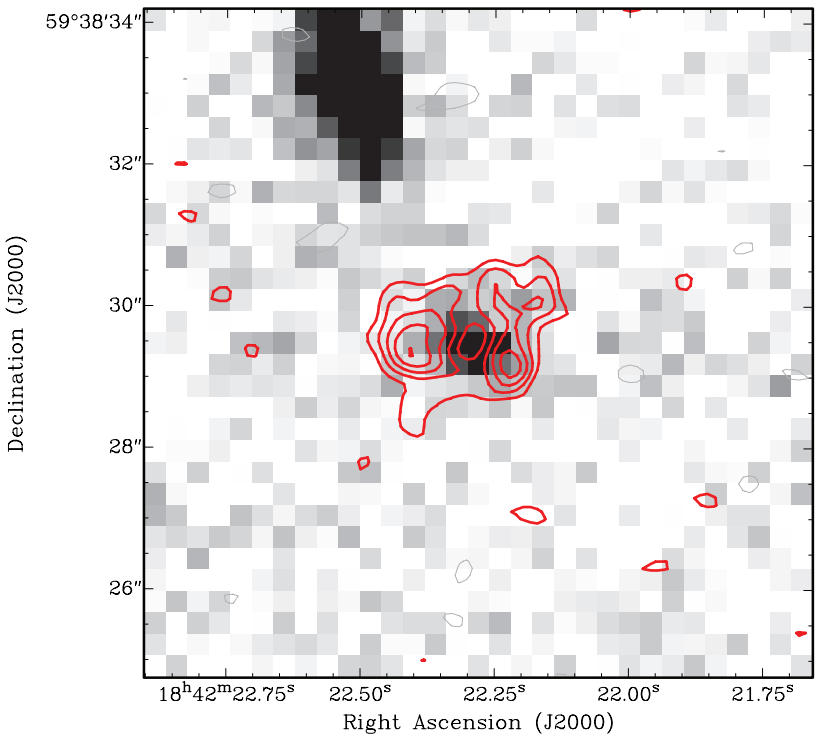

Figure 3. Overlay of the CO(2–1) contour map of MM18423+5938 and the *Ks*-band image of the main lens galaxy and N.E. nearby galaxy (gray scale). Contours are the same as in Figure 1 (right panel). Pixel size of the *Ks*-band image is 0.″304.

(A color version of this figure is available in the online journal.)

ring slightly ellipitical as observed but its mass and redshift cannot be separated with our current data. Had we derived its redshift, we could have speculated whether or not the *J*-band excess could be due to strong emission of its H_α line. The physical scale probed in the source with the beam of our EVLA map is $0.''6 \times (7.1\,\mathrm{kpc\,arcsec^{-1}})/\sqrt{m}$, i.e., 1.2 kpc with our first estimate of the magnification factor m.

We revise the far-IR luminosity $L_{\rm FIR}$ of MM18423+5938 given in Lestrade et al. (2010) since the strong *Spitzer* MIPS 70 μm source, tentatively associated with MM18423+5938 then, has now a position that is discrepant by more than 5σ with the more accurate EVLA position newly found for MM18423+5938. The SED of the dust emission was modeled by a single temperature modified blackbody function with the standard power law for the dust opacity, fitted to the available photometry at $\lambda = 1.2$, 2, and 3 mm given by Lestrade et al. (2010) and a 3σ upper limit of 3 mJy at 70 μm. We varied the opacity index over the range $1.0 < \beta < 2.0$ and the temperature over $20\,\mathrm{K} < T_{\rm dust} < 60$ K that are plausible for SMGs (e.g., Magnelli et al. 2010; Ivison et al. 2010; Hwang et al. 2010; Chapman et al. 2010), and found the range $2 \times 10^{13}\,m^{-1} < L_{\rm FIR} < 3 \times 10^{14}\,m^{-1}\,L_\odot$ with a 95% confidence level, where $L_{\rm FIR}$ is mostly the luminosity between $\lambda \sim 70\,\mu$m and 3 mm, and m is the magnification factor. Using the FIR to star formation rate conversion from Kennicutt (1998), this luminosity corresponds to a range in star formation rate of $3300\,m^{-1}\,M_\odot\,\mathrm{yr^{-1}} < \mathrm{SFR} < 22000\,m^{-1}\,M_\odot\,\mathrm{yr^{-1}}$. Recently, McKean et al. (2011) made a deep image at 1.4 GHz with the Westerbork array (WSRT) and detected MM18423+5938 at a position consistent with ours to within 1σ. They used the radio–FIR relation to infer an apparent luminosity $L_{\rm FIR} = 5.6^{+4.1}_{-2.4} \times 10^{13}\,L_\odot$ consistent with our new estimate.

The velocity-integrated CO(1–0) flux density yields a luminosity $L'_{\rm CO(1-0)} = 2.71 \pm 0.38 \times 10^{11}\,m^{-1}\,\mathrm{K\,km\,s^{-1}\,pc^2}$ using the relationships from Solomon et al. (1992). If corrected by $m \sim 12$, this is the typical luminosity found for SMGs, e.g., Harris et al. (2010), Frayer et al. (2011), and Ivison et al. (2011). This implies an H_2 mass of $2.2 \times 10^{11}\,m^{-1}\,M_\odot$ in assuming a CO(1–0) luminosity to H_2 mass conversion factor of $\alpha = 0.8\,M_\odot/\mathrm{K\,km\,s^{-1}\,pc^2}$, suitable for starburst galaxies in the nearby universe (Downes & Solomon 1998) and typically used for SMGs, e.g., Tacconi et al. (2008). The gas-to-dynamical mass ratio exceeds unity for the dynamical mass ($4.8 \times 10^{10}\,m^{-1}\,M_\odot$) computed for an hypothetical edge-on disk by using the FWHM of the lines ($\sim$200 km s^{-1}) as an indication of the rotation velocity. This exceedingly large ratio and the fact that a disk in MM18423+5938 is not expected to be supported by the radiation pressure of an AGN (Scoville et al. 1995) suggest that a disk would be inclined. Note that this ratio still exceeds unity if a merger model is used instead, the enclosed dynamical mass is approximately a factor of two larger in this case (Genzel et al. 2003). In Figure 1, the second component in the CO(1–0) and CO(2–1) lines detected at a low significance level is blueshifted by 200–300 km s^{-1}. We have verified that this component is not visible in the averaged profile of the three high-order ($J = 4$, 6, 7) CO lines observed at the IRAM 30 m (Lestrade et al. 2010), which indicates there are distinct CO components that have low excitation only within MM18423+5938. Such a component would be indicative of either a more extended low-order CO component of the rotating disk or possibly the second component of a merger.

The high-order CO excitation ladder observed with EMIR/IRAM was fitted with a large velocity gradient (LVG radiative transfer model, $T_k = 45$ K, $n(\mathrm{H_2}) = 10^3\,\mathrm{cm^{-3}}$, $N_{\rm CO}/\Delta V = 3 \times 10^{18}\,\mathrm{cm^{-2}/(kms^{-1})}$) in Lestrade et al. (2010). The CO(1–0) peak flux density (2.1 ± 0.2 mJy) is consistent with this model, while the CO(2–1) measurement (10.8 ± 2.2 mJy) is marginally in excess by $54\% \pm 30\%$ when the 20% calibration uncertainty

at 47 GHz is included. Although this uncertainty is presently large, we note that the ratio of the flux densities CO(2–1)/CO(1–0) is difficult to explain even with differential lensing if the excitation is spatially variable in the galaxy, unless CO(1–0) is moderately optically thick, with rising optical depth toward CO(2–1). New EVLA observations are required to investigate this in more detail.

The peak rest-frame brightness temperature of the ring is 12 K (east clump in our map of Figure 1). This is similar to what has been seen in other $z \sim 4$ SMGs, such as GN20 (Carilli et al. 2010), although we cannot rule out higher T_B clumps that are not resolved by our present observations.

4. CONCLUSIONS

While there is a long history of CO observations from strongly lensed, high-redshift galaxies (e.g., Alloin et al. 1997; Barvainis et al. 1994; Swinbank et al. 2010), MM18423+5938 is only the second complete Einstein ring seen in CO emission, after the $z = 4.1$ quasar host galaxy PSS J2322+1944 (Carilli et al. 2003). We identified the lens and derived a magnification factor of $\sim$12 using a preliminary lensing model. We measured a luminosity $L'_{\mathrm{CO}(1-0)}$, and corresponding H_2 mass, for MM18423+5938 that, when corrected for magnification, are similar to the unlensed SMGs. However, the relatively large range for L_{FIR} in our present analysis requires further observations to better sample the FIR SED in order to better constrain the implied star formation rate. As demonstrated by Riechers et al. (2008) for the molecular Einstein ring observed toward the QSO PSS J2322+1944, the brighter SMG MM18423+5938 provides a unique opportunity to study the gas dynamics on physical scale as small as $\sim$100 pc with further high sensitivity and high spatial resolution EVLA observations.

We acknowledge and sincerely thank Dr. S. D. J. Gwyn (CADC, Victoria, Canada) for promptly stacking the CFHT *Elixir* processed MegaCam data with *MegaPipe*. This work is based on EVLA observations conducted under the auspices of NRAO, WirCam and MegaCam observations conducted at CFHT, and on use of data products from the Two Micron All Sky Survey (2MASS).

Facilities: EVLA, CFHT

REFERENCES

Alloin, D., Guilloteau, S., Barvainis, R., Antonucci, R., & Tacconi, L. 1997, A&A, 321, 24
Arnouts, S., Cristiani, S., Moscardini, L., et al. 1999, MNRAS, 310, 540
Barvainis, R., Tacconi, L., Antonucci, R., Alloin, D., & Coleman, P. 1994, Nature, 371, 586
Bertin, E. 2006, in ASP Conf. Ser. 351, Astronomical Data Analysis Software and Systems XV, ed. C. Gabriel, C. Arviset, D. Ponz, & E. Solano (San Francisco, CA: ASP), 112
Bertin, E., & Arnouts, S. 1996, A&AS, 117, 393
Bertin, E., Mellier, Y., Radovich, M., et al. 2002, in ASP Conf. Ser. 281, Astronomical Data Analysis Software and Systems XI, ed. D. A. Bohlender, D. Durand, & T. H. Handley (San Francisco, CA: ASP), 228
Blain, A. W., Smail, I., Ivison, R. J., Kneib, J., & Frayer, D. T. 2002, Phys. Rep., 369, 111
Butler, B. J. 2010, EVLA Memo, 232 (http://www.vla.nrao.edu/memos/test)
Capak, P. L., et al. 2011, Nature, 470, 233
Carilli, C. L., & Holdaway, M. A. 1999, Radio Sci., 34, 817
Carilli, C. L., Lewis, G. F., Djorgovski, S. G., et al. 2003, Science, 300, 773
Carilli, C. L., Daddi, E., Riechers, D., et al. 2010, ApJ, 714, 1407
Chapman, S. C., Ivison, R. J., Roseboom, I. G., et al. 2010, MNRAS, 409, L13
Collins, C. A., Stott, J. P., Hilton, M., et al. 2009, Nature, 458, 603
Daddi, E., Dickinson, M., Chary, R., et al. 2005, ApJ, 631, L13
Downes, D., & Solomon, P. M. 1998, ApJ, 507, 615
Frayer, D. T., Harris, A. I., Baker, A. J., et al. 2011, ApJ, 726, L22
Genzel, R., Baker, A. J., Tacconi, L. J., et al. 2003, ApJ, 584, 633
Gwyn, S. D. J. 2008, PASP, 120, 212
Harris, A. I., Baker, A. J., Zonak, S. G., et al. 2010, ApJ, 723, 1139
Hwang, H. S., Elbaz, D., Magdis, G., et al. 2010, MNRAS, 409, 75
Ivison, R. J., Papadopoulos, P. P., Smail, I., et al. 2011, MNRAS, 412, 1913
Ivison, R. J., Swinbank, A. M., Swinyard, B., et al. 2010, A&A, 518, L35
Jullo, E., Kneib, J.-P., Limousin, M., et al. 2007, New J. Phys., 9, 447
Kennicutt, R. C., Jr. 1998, ApJ, 498, 541
Kneib, J.-P., Ellis, R. S., Smail, I., Couch, W. J., & Sharples, R. M. 1996, ApJ, 471, 643
Kotilainen, J. K., Falomo, R., Decarli, R., et al. 2009, ApJ, 703, 1663
Kriek, M., van Dokkum, P. G., Franx, M., et al. 2008, ApJ, 677, 219
Kurk, J., Cimatti, A., Zamorani, G., et al. 2009, A&A, 504, 331
Lestrade, J.-F., Combes, F., Salomé, P., et al. 2010, A&A, 522, L4
Lestrade, J.-F., Wyatt, M. C., Bertoldi, F., Menten, K. M., & Labaigt, G. 2009, A&A, 506, 1455
Magnelli, B., Lutz, D., Berta, S., et al. 2010, A&A, 518, L28
McKean, J. P., Berciano Alba, A., Volino, F., et al. 2011, MNRAS, 414, L11
Monet, D. G., Levine, S. E., Canzian, B., et al. 2003, AJ, 125, 984
Negrello, M., Hopwood, R., De Zotti, G., et al. 2010, Science, 330, 800
Perley, R. A., Chandler, C. J., Butler, B. J., & Wrobel, J. M. 2011, ApJ
Renzini, A. 2006, ARA&A, 44, 141
Riechers, D. A., Walter, F., Brewer, B. J., et al. 2008, ApJ, 686, 851
Riechers, D. A., Capak, P. L., Carilli, C. L., et al. 2010, ApJ, 720, L131
Scoville, N. Z., Yun, M. S., Brown, R. L., & Vanden Bout, P. A. 1995, ApJ, 449, L109
Skrutskie, M. F., Cutri, R. M., Stiening, R., et al. 2006, AJ, 131, 1163
Smail, I., Ivison, R. J., Blain, A. W., & Kneib, J. 2002, MNRAS, 331, 495
Solomon, P. M., Downes, D., & Radford, S. J. E. 1992, ApJ, 398, L29
Swinbank, A. M., Smail, I., Longmore, S., et al. 2010, Nature, 464, 733
Tacconi, L. J., Genzel, R., Smail, I., et al. 2008, ApJ, 680, 246
Toft, S., Franx, M., van Dokkum, P., et al. 2009, ApJ, 705, 255
van Dokkum, P. G., Franx, M., Kriek, M., et al. 2008, ApJ, 677, L5
Vieira, J. D., Crawford, T. M., Switzer, E. R., et al. 2010, ApJ, 719, 763
Williams, R. J., Quadri, R. F., Franx, M., van Dokkum, P., & Labbé, I. 2009, ApJ, 691, 1879